



Title	Kinetic analysis of workpiece rotation behavior during double-sided polishing
Author(s)	Satake, Urara; Seguchi, Yuta; Enomoto, Toshiyuki
Citation	CIRP Annals. 2025, 74(1), p. 435-439
Version Type	VoR
URL	https://hdl.handle.net/11094/102603
rights	This article is licensed under a Creative Commons Attribution 4.0 International License.
Note	

The University of Osaka Institutional Knowledge Archive : OUKA

<https://ir.library.osaka-u.ac.jp/>

The University of Osaka



Kinetic analysis of workpiece rotation behavior during double-sided polishing

Urara Satake, Yuta Seguchi, Toshiyuki Enomoto (1)*

Division of Mechanical Engineering, Graduate School of Engineering, Osaka University, 2-1 Yamada-oka, Suita, Osaka, Japan

ARTICLE INFO

Article history:
Available online 22 May 2025

Keywords:
Polishing
Modelling
Double-sided machining

ABSTRACT

Unique clamping mechanism adopted in double-sided polishing (DSP) enables free rotation of workpieces, which is critical for achieving uniform material removal. However, the DSP process has long faced the issue of non-rotating workpieces, resulting in tapered shapes—an issue particularly relevant to silicon wafer polishing. In this study, a kinetic analysis is conducted to investigate workpiece rotation during DSP and to clarify the mechanism underlying tapering. This analysis identifies key variables governing rotational speed and primary factors contributing to workpiece nonrotation. These findings are validated experimentally, and a practical approach to preventing tapering is proposed.

© 2025 The Author(s). Published by Elsevier Ltd on behalf of CIRP. This is an open access article under the CC BY license (<http://creativecommons.org/licenses/by/4.0/>)

1. Introduction

Double-sided polishing (DSP) is an effective method for achieving high-quality surface finishing on substrate materials. It serves as the current industry standard for silicon wafer finishing. A distinguishing feature of DSP is its unique workpiece clamping mechanism, wherein the workpiece is placed within a hole in a holder, referred to as a carrier, without being rigidly clamped. This design prevents clamping-induced stress on the workpiece, which is an essential advantage for substrate materials prone to stress-related deformation. Another advantage of this loose holding arrangement is that the workpiece is not restricted by the deterministic kinematics of the carrier's planetary motion. Instead, it can rotate freely within the carrier's hole. This rotation is critical for ensuring uniform material removal across its surface. In the context of DSP, the inherent geometry and kinematics [1] induce slight nonuniformities in material removal along the workpiece diameter during each carrier rotation. As the workpiece rotates, these nonuniformities vary with each carrier rotation. They effectively compensate for each other throughout the process, resulting in negligible overall nonuniformity. In contrast, if the workpiece does not rotate, mostly identical nonuniformity patterns emerge during each carrier rotation, resulting in workpiece tapering. This tapering is particularly problematic for silicon wafers, as it adversely impacts lithography throughput in semiconductor manufacturing [2]. However, the DSP process has long faced the issue of workpieces remaining not rotating.

To address this issue, numerous studies have focused on improving the understanding of workpiece rotation. Notably, during DSP, the workpiece is positioned between the upper and lower platens. This configuration reduces workpiece visibility and limits the application of established techniques used for measuring workpiece rotation in other processes [3,4]. Researchers have attempted direct observations by replacing the upper platen with a transparent acrylic plate [5] or omitting the upper platen

entirely [6]. The corresponding results have revealed continuous variations in rotation, which is a critical factor influencing material removal uniformity. However, these methods are constrained by their reliance on setups that deviate from standard DSP configurations. To overcome these limitations, a new approach has been recently proposed [7,8]. This method involves determining the rotational speed by measuring the displacement of marks on the workpiece during short-duration processes. However, this method only provides average rotational speed, failing to capture the continuous variations. To address these experimental challenges, researchers have turned to numerical approaches. A pioneering analytical model determined rotational speed by analyzing the equilibrium of torques generated by frictional forces at the interface with polishing pads [9]. This model was later refined to include frictional forces at the interface with the carrier, enabling it to represent continuously varying rotation [10]. A comparable model was subsequently presented in [7].

The analytical models are well established. However, prior research has primarily focused on predicting workpiece rotation rather than thoroughly examining the underlying rotational behavior. The mechanisms responsible for the frequent nonrotation of workpieces remain unknown, hindering the development of effective strategies to prevent workpiece tapering. This research employs an analytical model to elucidate the characteristics of workpiece rotation during DSP, rather than solely predicting rotational speeds. The obtained findings are applied to identify the process variables influencing rotational behavior and to clarify the mechanisms underlying tapered workpiece formation. The validity of these results is verified through rotational speed measurements conducted with a newly developed system, along with polishing experiments on silicon wafers. Based on these findings, this study also proposes a practical method to eliminate tapering in DSP processes.

2. Workpiece rotation behavior

During a DSP process (Fig. 1(a)), the polishing pads exert frictional forces on the workpiece surface, which generate torques that induce

* Corresponding author.

E-mail address: enomoto@mech.eng.osaka-u.ac.jp (T. Enomoto).

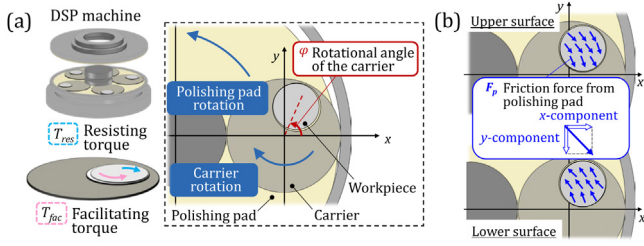


Fig. 1. (a) Schematic of the DSP process and (b) friction force F_p .

workpiece rotation. These forces also press the workpiece against the carrier. An additional frictional force develops at the interface between the workpiece and the carrier, generating a torque that opposes the workpiece's rotation. The rotational speed of the workpiece (ω_w) is governed by the following equation of motion:

$$I \frac{d\omega_w}{dt} = T_{fac} + T_{res} \quad (1)$$

where I represents the moment of inertia of the workpiece, and t denotes time. T_{fac} represents the sum of the torques generated by frictional forces at the interface with the polishing pads, which facilitate the workpiece's rotation. T_{res} denotes the torque generated by the frictional force at the carrier interface, which resists the workpiece's rotation. Fig. 2(a) shows the workpiece's rotational speed calculated under the polishing conditions listed in Table 1, which are typical for the DSP of silicon wafers. The vertical line represents the workpiece's rotational speed relative to the carrier's rotational speed (ω_w^*), which is referred to as the workpiece's rotational speed in this paper. The workpiece's rotational speed displays specific characteristics consistent with prediction results reported in the literature [10]:

- The workpiece rotates in the opposite direction to the carrier, exhibiting periodic variations based on its position, which is defined by the rotational angle of the carrier, φ (see Fig. 1(a)).
- The rotational speed peaks at $\varphi = 180^\circ$ and decreases at positions between $\varphi = 0^\circ$ and $\varphi = 180^\circ$, as well as between $\varphi = 180^\circ$ and $\varphi = 360^\circ$.

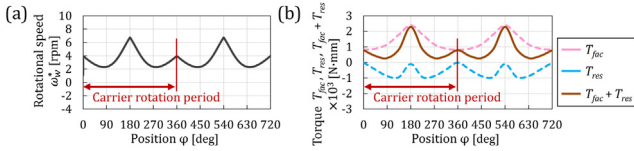


Fig. 2. (a) Workpiece rotational speed and (b) torques.

Table 1
Polishing conditions used in calculations.

Dimension	[mm]
Workpiece diameter	300
Inner gear diameter	751
Carrier diameter	700
Distance between workpiece and carrier	182.5
Rotation	[rpm]
Upper polishing pad	-17
Lower polishing pad	17
Carrier	-5
Friction coefficient	
Workpiece-Polishing pad	0.16
Workpiece-Carrier μ_c	0.15

Speed is relative to carrier revolution.

To enhance the understanding of these characteristics, this study focuses on the facilitating torque (T_{fac}) and the resisting torque (T_{res}). Eq. (1) indicates that variations in the workpiece's rotational speed can be predicted from changes in the sum of these torques, as confirmed in Fig. 2(b). Although these torques have opposing effects on rotation, both are influenced by the friction forces exerted by the polishing pads (F_p) (Fig. 1(b)). T_{fac} represents the sum of the torques from the F_p forces at every position on the workpiece, while T_{res} is directly proportional to the resultant force of these F_p forces. Analyzing the impact of the F_p forces on each torque will provide valuable insights into rotational behavior.

The direction of the F_p force can vary, which in turn affects its x- and y-components, where x and y represent the radial and tangential

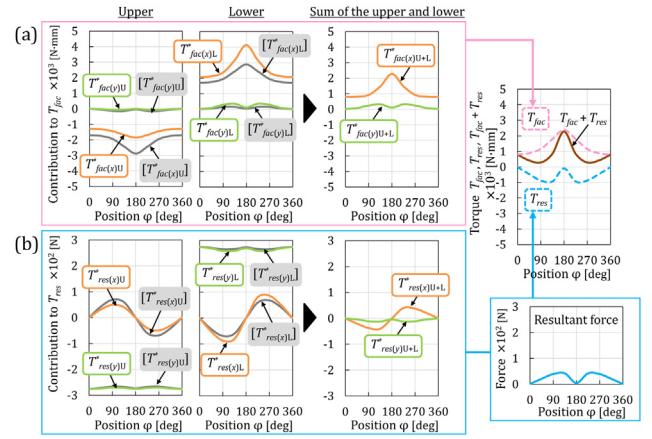


Fig. 3. Contributions of the x- and y-components to (a) T_{fac} and (b) T_{res} .

directions, respectively. Fig. 3(a) shows the contributions of the x- and y-components to the facilitating torque ($T_{fac(x)}$ and $T_{fac(y)}$) during one carrier rotation, and Fig. 3(b) shows their contributions to the resisting torque ($T_{res(x)}$ and $T_{res(y)}$). Subscripts "U", "L", and "U+L" signify the contributions from the upper and lower surfaces of the workpiece, as well as the sum of these contributions. The gray line represents each contribution when the carrier does not rotate (i.e., only the polishing pads rotate), indicated with brackets (e.g., $[T_{fac(x)}]_U$). In this scenario, the F_p forces acting on the upper and lower surfaces are always opposing due to the opposing rotation of the upper and lower polishing pads, leading to the complete cancellation of each contribution. This highlights the critical role of carrier rotation in influencing torque dynamics and, consequently, the workpiece's rotation. Comparing scenarios with and without carrier rotation reveals that the y-component contributions ($T_{fac(y)}$ and $T_{res(y)}$) remain largely unchanged, while the x-component contributions ($T_{fac(x)}$ and $T_{res(x)}$) undergo notable changes due to carrier rotation. Carrier rotation changes the direction of the relative velocity between the workpiece and the polishing pads, thereby altering the direction of the F_p forces. In the context of DSP, where the polishing pad is significantly larger than the workpiece and the carrier, the y-component of F_p remains largely unchanged, even as the direction of F_p varies. Conversely, the x-component is more direction-sensitive: It increases on a surface where the polishing pad rotates opposite to the carrier and decreases on that where both rotate in the same direction. This relationship explains the results presented in Fig. 3. Compared to the scenario with a nonrotating carrier, the x-component contributions increase on the lower workpiece surface, where the polishing pad rotates opposite to the carrier in the examined conditions (see Table 1). Conversely, they decrease on the upper workpiece surface, where both rotate in the same direction. As a result, an imbalance arises between the upper and lower surface contributions, preventing their cancellation. The workpiece's rotation is affected by the contributions that remain uncanceled ($T_{fac(x)U+L}$ and $T_{res(x)U+L}$). The characteristics shown in Fig. 2(a) can be explained as follows:

- The residual $T_{fac(x)U+L}$ aligns with $T_{fac(x)}$ on the surface where the polishing pad rotates opposite to the carrier, causing the workpiece to rotate in the opposite direction to the carrier.
- At $\varphi = 180^\circ$, $T_{fac(x)}$ peaks, while $T_{res(x)}$ is zero. Consequently, the workpiece's rotational speed reaches its peak.
- $T_{res(x)}$ peaks around $\varphi = 120^\circ$ and 240° , leading to the reduction in the workpiece's rotational speed at positions between $\varphi = 0^\circ$ and $\varphi = 180^\circ$, as well as between $\varphi = 180^\circ$ and $\varphi = 360^\circ$.

In summary, the carrier-rotation-induced imbalance in the x-components of the F_p forces between the upper and lower surfaces significantly influences workpiece rotation. Thus, the magnitude and direction of the carrier's rotational speed are critical for effectively controlling the workpiece's rotation.

3. Workpiece tapering

3.1. Mechanism of workpiece tapering

A workpiece tapers when it does not rotate, which occurs when the resisting torque (T_{res}) exceeds the facilitating torque (T_{fac}). Fig. 4

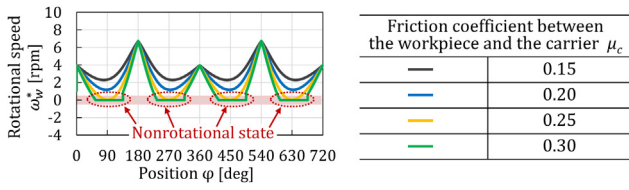


Fig. 4. Effects of μ_c on workpiece nonrotation.

illustrates the workpiece rotational speeds calculated for different values of the frictional coefficient (μ_c) between the workpiece and the carrier. Workpiece nonrotation is more likely at higher μ_c values because T_{res} is directly proportional to this coefficient.

Notably, workpiece tapering occurs only when it remains in a nonrotational state throughout the carrier rotation. However, T_{res} approaches zero at $\varphi = 0^\circ$ and 180° (as shown in Fig. 2(b)), making nonrotational states unlikely at these positions, no matter how high the μ_c value is. To clarify the tapering mechanism, scenarios in which T_{res} does not approach zero, even at these positions, must be identified. In the normal scenario detailed in Section 2, the y-component imbalance between the upper and lower surfaces is negligible, resulting in almost complete cancellation of $T_{res(y)}$, as shown in Fig. 3(b). This suggests that a failure in the normal scenario could result from limited cancellation of $T_{res(y)}$, caused by an imbalance in the y-components of F_p acting between the upper and lower surfaces. Such an imbalance may arise from differences between the friction coefficients at the workpiece–upper polishing pad interface ($\mu_{p,U}$) and the workpiece–lower polishing pad interface ($\mu_{p,L}$). Fig. 5 shows the calculation results for the scenario where $\mu_{p,U}$ (0.16) is higher than $\mu_{p,L}$ (0.13). When $\mu_{p,U}$ equals $\mu_{p,L}$ (Fig. 3(b)), the magnitudes of $T_{res(y)}$ on the upper and lower surfaces are comparable, leading to almost complete cancellation. Conversely, when $\mu_{p,U}$ and $\mu_{p,L}$ differ, the disparity in $T_{res(y)}$ magnitudes limits cancellation (Fig. 5(a)). As a result, T_{res} is likely to exceed T_{fac} (Fig. 5(b)), resulting in prolonged nonrotation (Fig. 5(c)). This can cause the workpiece to remain nonrotational throughout the carrier rotation, leading to its tapering.

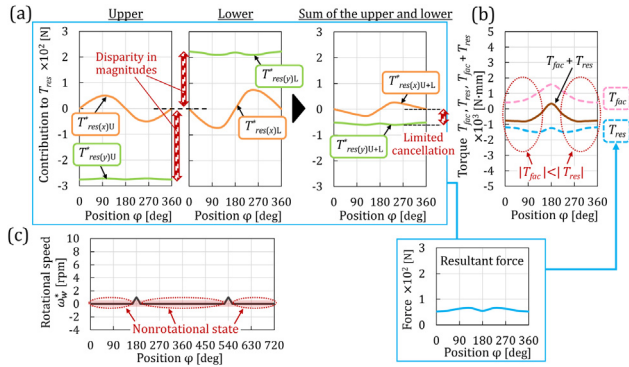


Fig. 5. (a) Contributions to T_{res} , (b) torques, and (c) workpiece rotational speed when $\mu_{p,U}$ (0.16) is higher than $\mu_{p,L}$ (0.13).

3.2. Approach to preventing workpiece tapering

Minimizing the difference between the friction coefficients of the upper ($\mu_{p,U}$) and lower ($\mu_{p,L}$) surfaces is an effective strategy for preventing workpiece tapering. However, achieving this in practice is challenging owing to variations in lubrication conditions between the surfaces, primarily caused by the supply of the slurry only from the upper side. Furthermore, variations in the surface conditions of polishing pads, primarily attributed to wear and clogging, can exacerbate the difference between $\mu_{p,U}$ and $\mu_{p,L}$. This study proposes a method to mitigate workpiece tapering, even when $\mu_{p,U}$ and $\mu_{p,L}$ differ considerably.

One potential solution involves increasing the facilitating torque by increasing the y-component contribution to this torque ($T_{fac(y)}$), which is consistently minimal in the conventional scenario, as shown in Fig. 3(a). Importantly, even brief rotations at specific workpiece positions (φ) can effectively prevent tapering. Among the positions, $\varphi = 180^\circ$ is the most effective for inducing rotation, as $T_{fac(x)}$ peaks at this position. Thus, this study specifically focuses on increasing $T_{fac(y)}$ at $\varphi = 180^\circ$. As illustrated in Fig. 6(a), the small $T_{fac(y)}$ at $\varphi = 180^\circ$ results from the cancellation of torques acting on the left and right halves of the workpiece surface.

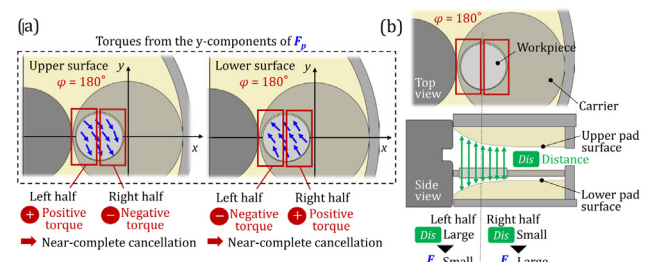


Fig. 6. (a) Torque cancellation at $\varphi = 180^\circ$ and (b) proposed approach.

Suppressing this cancellation would increase $T_{fac(y)}$ on both the upper and lower surfaces. Moreover, in the investigated scenario (i.e., $\mu_{p,U}$ and $\mu_{p,L}$ are different), $T_{fac(y)}$ values on the upper and lower surfaces do not completely cancel each other out due to their differing magnitudes, increasing $T_{fac(y)U} + T_{fac(y)L}$.

This suppression can be achieved by varying the F_p force applied to the left and right halves of the workpiece. One approach is to use non-parallel upper and lower polishing pads with specially designed surfaces (Fig. 6(b)). The F_p force applied at a specific point on the workpiece can be increased by decreasing the distance between the upper and lower polishing pad surfaces (Dis) at that point [11]. Thus, varying Dis between the left and right halves of the workpiece could effectively adjust the F_p force. A practical example involves grinding the innermost sections of the polishing pads, increasing Dis on the left half of the workpiece at $\varphi = 180^\circ$.

4. Experimental analysis

4.1. Experimental procedure

The experiments were conducted to validate the theoretical findings (Fig. 7). The experiments utilized a DSP machine (HAMAI 9BF), stainless steel carriers, and 5-in silicon wafers. To overcome visibility limitations during DSP, workpiece rotational speed was evaluated using a mock wafer made of two silicon wafers with an acrylic foam plate between them. The thicker mock wafers (42 mm) compared to standard silicon wafers facilitated side-mark observations during processing, allowing us to capture continuously varying rotational speeds. The lightweight acrylic foam minimized discrepancies in moment of inertia compared to actual silicon wafers. Mock wafer components used silicon wafers with relatively rough surfaces (Sa: 360 nm) to match pre-DSP conditions. Seven experimental conditions (C1–7) were tested (Table 2). C1–3 were used to examine the effect of carrier rotational speed. In C4 and C5, a silicon wafer with a lower surface roughness (Sa: 10 nm) replaced the lower and upper mock wafer components, respectively, to create friction coefficient differences between the upper and lower surfaces. In C1–5, the carrier revolution speed was fixed at zero to enable the use of an external camera, ensuring data stability. C6 and C7 included carrier revolution to simulate subsequent polishing tests, with a camera mounted onto the carrier. C1–6 used polyurethane polishing pads as both the upper and lower polishing pads. In C7, a polyurethane pad was used as the upper polishing pad, while a nonwoven pad was used as the lower polishing pad to create friction coefficient differences. Each experimental condition was tested twice.

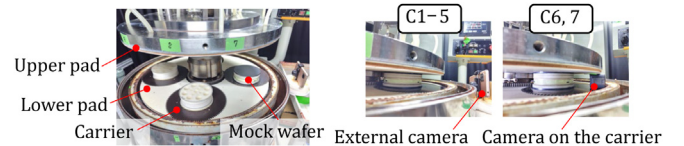
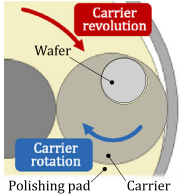


Fig. 7. Setup for evaluating workpiece rotational speed.

The friction coefficient was evaluated for three contact interfaces: a rough wafer–polyurethane polishing pad, a low-roughness wafer–polyurethane polishing pad, and a rough wafer–nonwoven polishing pad. Friction force was measured using load cells in a single-sided polishing setup. Measurements were taken at polishing pad rotational speeds of 10–40 rpm under a constant pressure of 13.8 kPa. Each measurement was taken three times. Polishing tests were conducted to

Table 2
Polishing conditions used in experiments.

Condition	C1	C2	C3–5	C6, 7
Rotation [rpm]				
- Upper polishing pad		8.3		10
- Lower polishing pad		–25		–30
- Carrier	–11	–17	–23	–16.4
Carrier revolution [rpm]		0		–6.5
Pressure [kPa]		9.0		13.8



compare the performance under C6 and C7. A colloidal silica slurry containing 1.0 wt% abrasive particles was supplied at a rate of 2 l/min. The target stock removal was set at 15 μm , and five wafers were polished under each condition. Before testing, each wafer had an approximate thickness of 530 μm and showed a nearly uniform thickness distribution. The thickness profiles of three wafers, which achieved close to 15 μm of stock removal, were measured after each test using a spectral interferometric film thickness instrument (Otsuka Electronics SF3/300). Tapering was evaluated along sixteen different diameter directions. The maximum thickness difference between two points located 108 mm apart on each line was used as the tapering index.

4.2. Results and discussion

Fig. 8 shows the variation in wafer rotational speed over two carrier rotations under C1–5. Consistent with the kinetic analysis, the wafer rotates opposite to the carrier, with its rotational speed peaking at $\varphi = 180^\circ$. The maximum wafer rotational speed increases with carrier rotational speed (Fig. 8(a)). The facilitating torque (T_{fac}) and resisting torque (T_{res}) result from frictional imbalances between the upper and lower surfaces, caused by the carrier rotation. Increasing the carrier rotational speed raises both torques. At $\varphi = 180^\circ$, T_{res} is zero regardless of the carrier rotational speed (see Fig. 3), allowing the increased T_{fac} to enhance the workpiece rotational speed. As outlined in Section 3.1, workpiece tapering can be prevented as long as the workpiece does not remain in a nonrotational state. However, if the workpiece rotates at a too-low speed, the risk of tapering increases. A higher carrier rotational speed is desired to minimize this risk, as it helps ensure a nonzero workpiece rotational speed with a safer margin.

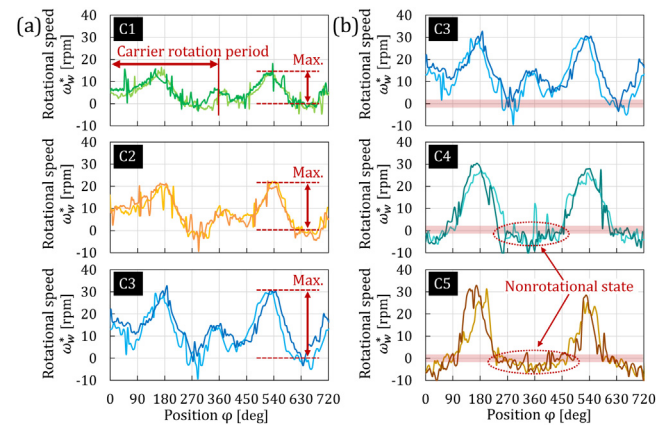


Fig. 8. Wafer rotational speed in (a) C1–3 and (b) C3–5.

As indicated in Fig. 9, the friction coefficients on the upper and lower surfaces differ in C4 and C5 compared to those in C3. The nonrotational state lasted longer in C4 and C5, with the longest duration observed in C5 (Fig. 8(b)). As detailed in Section 2, carrier rotation induces a discrepancy in the x-component of the F_p force acting between the upper and lower surfaces. Specifically, the x-component increases on the surface (Sur-A) where the polishing pad and the carrier rotate in opposite directions, and decreases on the opposing surface (Sur-B). This discrepancy enhances workpiece rotation. In scenarios where the friction coefficient is higher on Sur-B, as in C5, the x-component on Sur-B increases due to higher friction coefficient. This increase reduces the discrepancy caused

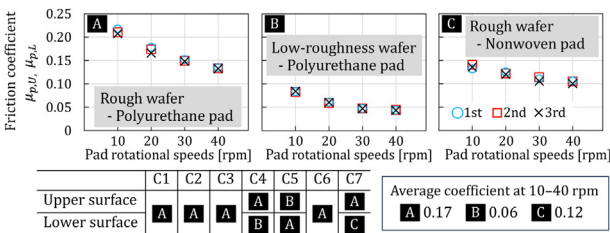


Fig. 9. Results of friction coefficient measurements.

by carrier rotation, hindering workpiece rotation. This is why C5 had a more prolonged nonrotational state than C4.

Similarly, friction coefficient measurements (Fig. 9) reveal differences between the upper and lower surfaces in C7 compared to C6. As shown in Fig. 10(a), the wafer stayed nonrotational throughout the process under C7, whereas C6 showed slight rotation. Fig. 10(b) shows the tapering index. The tapering index measurements had an uncertainty of ± 103 nm. C7 exhibited more tapering effects than C6, confirming the tapering mechanism found in the kinetic analysis. This verified the desirability to minimize the friction coefficient difference between the upper and lower surfaces to prevent workpiece tapering.

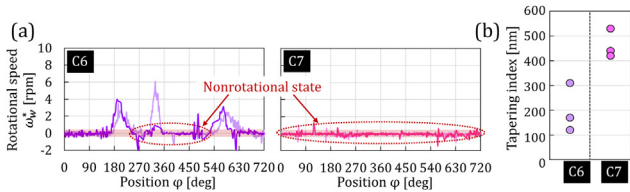


Fig. 10. (a) Wafer rotational speed and (b) wafer tapering in C6 and C7.

5. Conclusion

In DSP processes, workpiece tapering occurs when the workpiece does not rotate. Kinetic analysis highlights the critical role of carrier rotation in creating friction force imbalances between the upper and lower surfaces of the workpiece, which generate the torques required for workpiece rotation. The rotational speed of the carrier is thus a key variable for controlling the rotational speed of the workpiece. The behavior of workpiece rotation—its opposite direction to carrier rotation and periodic speed variations—is governed by rotational dynamics. The primary cause of workpiece nonrotation is the difference in friction coefficients between its interfaces with the upper and lower polishing pads. Theoretical findings are validated through rotational speed evaluations and DSP experiments on silicon wafers using a newly designed system for improved rotational speed measurement. To prevent tapering, minimizing the friction coefficient differences between the upper and lower workpiece surfaces is essential yet practically challenging. An alternative approach involves creating friction force imbalances on the left and right halves of the workpiece, achievable using polishing pads with nonparallel surfaces. Future research should verify this approach experimentally and explore the impact of friction coefficient variations, including their nonuniformity across polishing pads and their dependency on relative speed, on workpiece rotation.

Declaration of competing interest

The authors declare that they have no known competing financial interests or personal relationships that could have appeared to influence the work reported in this paper.

CRediT authorship contribution statement

Urara Satake: Writing – original draft, Software, Methodology, Investigation, Conceptualization. **Yuta Seguchi:** Methodology, Investigation. **Toshiyuki Enomoto:** Writing – review & editing, Methodology, Investigation.

References

- [1] Uhlmann E, Ardelt T, Spur G (1999) Influence of kinematics on the face grinding process on lapping machines. *CIRP Annals* 48(1):281–284.
- [2] Ruan J, Hartley J (2008) An innovative design of wafer height and tilt sensor for lithography systems. *Journal of Vacuum Science & Technology B* 26:2043–2048.
- [3] Yang Y, Li H, Liao Z, Axinte D (2019) A curious observation of phenomena occurring during lapping/polishing processes. *Proceedings of the Royal Society A* 475 (2230).
- [4] Dražumerić R, Badger J, Gustavsson T, Krajnik P (2022) Mechanics of self-rotating double-disc grinding process. *CIRP Annals* 71(1):309–312.
- [5] Suwabe H, Kamimura T, Ishikawa K (2022) Study on factors affecting wafer actions during double-sided lapping. *Journal of the Japan Society for Abrasive Technology* 66(9):524–529.
- [6] Hashimoto Y, Sano T, Furumoto T, Hosokawa A (2019) Development an identification method of friction coefficient between wafer and carrier in double-sided lapping. *Precision Engineering* 56:364–369.
- [7] Pan B, Kang R, Zhu X, Du D, Huang W, Guo J (2022) Formation mechanism of concave and convex surface shapes in double-sided lapping. *Journal of Materials Processing Technology* 309:117749.
- [8] Yang L, Guo X, Kang R, Zhu X, Jia Y (2022) Effect of kinematic parameters considering workpiece rotation on surface quality in YAG double-sided planetary lapping with the trajectory method. *The International Journal of Advanced Manufacturing Technology* 123:2679–2690.
- [9] Nakagawa Y (2006) Optimization of double sided polishing conditions in order to unify friction distance distribution in a wafer. *Journal of the Japan Society of Precision Engineering* 72(5):641–646.
- [10] Hashimoto Y, Kondo R, Furumoto T, Hosokawa A (2017) Development of highly accurate simulation model of wafer behavior considering contact between wafer and carrier during double-sided lapping. *Journal of the Japan Society for Precision Engineering* 83(5):433–438.
- [11] Satake U, Enomoto T (2023) Polishing pad design for uniform removal distributions in double-sided Polishing. *CIRP Annals* 72(1):289–292.